VYSOKÉ UČENÍ TECHNICKÉ V BRNĚ

BRNO UNIVERSITY OF TECHNOLOGY

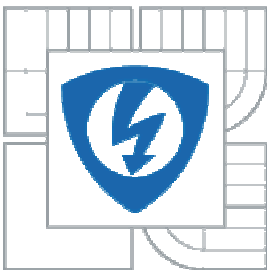

FAKULTA ELEKTROTECHNIKY A KOMUNIKAČNÍCH TECHNOLOGIÍ

ÚSTAV RADIOELEKTRONIKY

FACULTY OF ELECTRICAL ENGINEERING AND COMMUNICATION

DEPARTMENT OF RADIO ELECTRONIC

(SUB)MILLIMETER-WAVE ANTENNAS

ANTÉNY PRO PÁSMO (SUB)MILIMETROVÝCH VLN

SHORT VERSION OF DOCTORAL THESIS

ZKRÁCENÁ VERZE DIZERTAČNÍ PRÁCE

AUTHOR **KAMIL PÍTRA**

AUTOR PRÁCE

SUPERVISORS **Prof. ZBYNĚK RAIDA**

VEDOUCÍ PRÁCE **Prof. HANS LUDWIG HARTNAGEL**

BRNO 2014

KLÍČOVÁ SLOVA

Terahertzová anténa, terahertzový zdroj, dvojštěrbinová anténa, struktura s elektromagnetickým zádržným pásmem (EBG), hříbková EBG struktura, částečně odrazný povrch (PRS), planární čočka.

KEYWORDS

THz antenna, THz source, dual-slot antenna, electromagnetic band gap structure (EBG), mushroom-like EBG, partially reflective surface (PRS), planar lens.

MÍSTO ULOŽENÍ PRÁCE

Vědecké oddělení, FEKT VUT v Brně, Technická 3058/10, 602 00 Brno

STORAGE PLACE

Research department, FEEC BUT, Technická 3058/10, 602 00 Brno

ACKNOWLEDGEMENT

SIX research centre
sensor, information and communication systems

The research described in my thesis was performed in laboratories of the SIX Research Center, the registration number CZ.1.05/2.1.00/03.0072, the operational program Research and Development for Innovation.

CONTENTS

1 INTRODUCTION

With wavelengths between $\lambda = 1000 \div 300$ μm (300 GHz to 10 THz), the terahertz range bridges the gap between microwave region and infra-red frequencies, being until recently one of the least explored regions of the electromagnetic spectrum. In this text the THz range is defined as a frequency range from 300 GHz to 3 THz (as defined in [1]).While both sides of the spectrum, optics and electronics, have a long history of research and development, leading to a huge amount of commercially available sources, detectors and many additional devices, the THz range is still in its beginnings. The reason for this might be an absence of practical sources of THz radiation. The delayed development is mainly due to the difficulty of producing reliable THz-wave generators delivering sufficient output power as well as sensors that can detect this radiation.

For about 20 years (1970-1990), high-resolution spectroscopy and remote sensing of the Earth were the only driving forces for THz science [3]. Based on heterodyne and Fourier transform techniques, these methods offered astronomers, chemists and space scientists a tool for investigating the thermal emission lines of a wide diversity of light-weight molecules, as approximately one-half of the total luminosity and 98% of the photons emitted since the Big Bang have fallen into the submillimeter and far-infrared (P. Siegel, Jet Propulsion Laboratory) [4], [5], [6]. The THz frequency range is therefore frequently described as the "most scientifically useful yet least explored" [2].

Besides the rather traditional scientific application areas a large amount of other applications can also utilize the unique properties of the THz-wave region. Many new applications could be identified and some of them have a high commercial potential in the future. During the last decade, the general interest in THz radiation rose, mainly due to its ability to penetrate many organic materials, without the damage associated with ionizing radiation like X-rays. Since THz radiation is strongly absorbed by water molecules, it can be used to discernment between materials with varying water content. All these properties laid the basics for extensive applications in process and quality control [7] like biomedical imaging (T-ray imaging) [8]. Tests are currently under way to determine whether terahertz tomographic imaging can augment or replace mammography [9], and some scientists have proposed terahertz imaging as a method of screening passengers for explosives, weapons at airports [10]. By analyzing the frequency dependence of the transmission or reflection intensity, each substance has a unique behavior, so called "Fingerprinting" that is assigning a spectral characteristic to each molecule or chemical [11]. One of the amazing properties of THz radiation is its ability to pass through a wide range of materials, making it possible to "see" through many materials such as paper, cardboard, textiles, plastics, wood and etc. This property allows nondestructive and noninvasive inspection of mail packages and envelopes in post offices, luggage and personal belongings in airports, border crossing points and etc. This is the reason why the THz-waves can be used in security applications.

2 STATE-OF-THE-ART

The research is dominantly aimed to develop broadband and high efficiency continuous wave (CW) THz sources that can be used in compact semiconductor-based transmitter and receiver blocks. The general requirements cover low costs, tunability, small size, robustness and high spectral purity. High spectral purity can be ensured by CW sources which can produce output signals with a narrow line width over a broad frequency range [2].

The THz source generating submillimeter wave radiation is the key element of the integrated emitter/receiver. We therefore review different concepts of THz sources. The review comprises CW semiconductor photomixers and semiconductor diodes for CW THz generation [2], [12]. The review covers:

- Terahertz wave generation [2], [13];
- Photomixing [2], [14];
- Photoconductive mixers [2], [15], [16];
- p-i-n diodes [2], [17];
- Optical waveguide coupled photodiodes [2], [18];
- Optical rectification [2], [19];
- Surface emitters [20], [21];
- Uni-traveling carrier photodiode [22], [23].

2.1 Antennas for Integrated Photomixers

In general, integrated photomixers consist of a planar antenna and a hemispherical lens. The antenna is printed on the same substrate layer as the photomixer device. The lens is placed on the backside of the substrate layer. The lens is typically made of silicon [15].

Two antenna concepts can be applied when integrating with photomixers:

- Narrowband, resonant antenna structures;
- Broadband, frequency independent antennas.

In the thesis, a narrowband, resonant concept is applied.

When deciding about a specific antenna structure, the antenna impedance (input impedance), the radiation pattern, the polarization and the radiation efficiency are most important parameters to be considered.

Input impedance of resonant antennas is closely related to the frequency. Narrowband antennas exhibit a higher gain compared to broadband antennas. This is the main motivation for designing a resonant antenna. Since the output power of available THz sources is very low [2], [15], exploitation of a resonant antenna is the first issue, and correct impedance matching between the device and the antenna is the second issue.

The input resistance of the antenna might be satisfactorily high even if the antenna operates out of resonance [24], [25], [26]. In order to compensate the reactance of the device, we design an antenna out of the resonance.

Typical structures of narrowband resonant antennas to be potentially applied are:

- The dipole geometry [27];
- The dual-dipole geometry [27];
- The slot geometry [27];
- The dual slot geometry [22].

The conventional narrowband antennas for photoconductive mixers have the following fundamental properties:

- Linear polarization is produced;
- Dimensions correspond with the wavelength;
- Silicon lens is used for focusing radiated power;
- The radiating element exhibits lower gain;
- Side lobes are of a high level;
- Dimensions of the device are large due to a silicon lens.

For future security applications, the conventional narrow band antennas are not suitable since any antenna element has to be completed by a silicon lens to focus a beam. This work is aimed to create a multilayer planar structure supporting circular polarization. Therefore, the silicone lens is requested to be replaced by a purely planar structure called partially reflecting surface (PRS or superstrate). PRS has not been published in the field of THz technologies yet. PRS can be used for narrow-band structures only due to narrowband characteristics of the superstrate (PRS) and a narrowband axial ratio (about 3 %).

2.2 Objectives

Here, we formulate main objectives of the dissertation thesis and summarize all challenges resulting from investigated problems.

Objective 1:

- *To propose a design procedure for circularly polarized antennas operating at (sub)millimeter-wave frequencies*

The main objective can be divided into three sub-goals:

- *To replace a silicone lens by a partially reflecting surface (PRS);*
- *To exploit photoconductive mixers for the excitation of an antenna operating at THz frequencies with circular polarization;*
- *To verify a requested high directivity and a wide axial ratio of the device experimentally.*

The work is aimed to propose a design procedure for a planar multilayer THz source exhibiting a circular polarization. Properties of such a source are going to be improved using a planar superstrate (PRS) (improving gain) and a mushroom-like EBG structure (suppressing surface waves, reducing sidelobe level). The design procedure can be used for narrow-band structures only due to narrowband characteristics of the superstrate and narrowband axial ratio.

3 NOVEL MULTI-LAYER THZ SOURCE

3.1 Circular polarization

A THz system with linear antennas both in a receiver and in a transmitter should keep the polarization plane unchanged for the best transmission. The fixed polarization plane can be kept in static applications (detection). But in security applications, the position of a hidden object can continuously move, rotate, etc. In a linearly polarized system, a polarization misalignment of 45° degrades the signal for up to 3 dB, and the misaligned of 90° attenuates the signal up to 20 dB. The circularly polarized THz is immune against changes of the polarization plane. So, the quality of the detection stays perfect in all the cases. Structure of the proposed THz source is shown in Fig. 3.1.

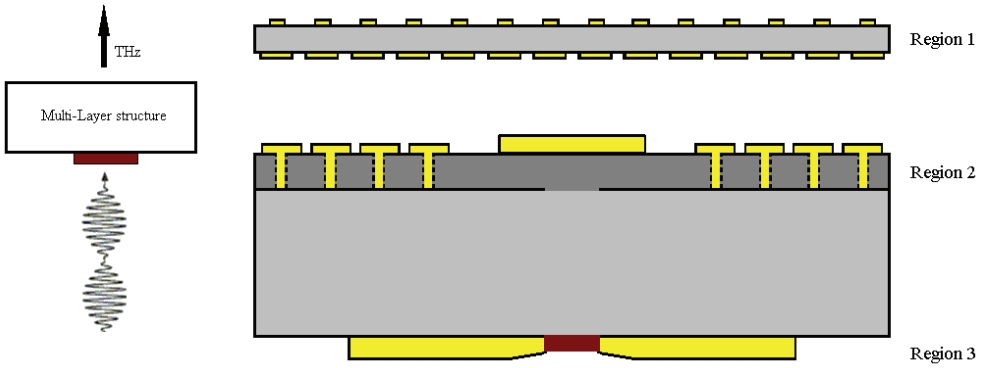

Fig. 3.1: Sketch of the proposed THz source.

The proposed THz antenna consists of three regions:

- Region 1: A partially reflective surface (a planar lens, a Fabry-Perot resonator);
- Region 2: A THz antenna with crossed slots and a mushroom-like EBG structure;
- Region 3: A photoconductive photomixer and a dual-slot antenna and a DC biasing.

In order to generate a circularly polarized wave, two laser sources are combined and focused on the photomixer. The resulting THz-modulated current is forwarded into an antenna [2], which emits CW THz radiation (emission) into surrounding space [2], [25], [26]. The THz emission passes through the (GaAs) substrate and irradiates the cross slots with different lengths which generate circular polarization. The multi-layer source requires a square patch on the top of the structure to achieve two orthogonal modes for CP operation (TM_{10} and TM_{01}). Obviously, the resonant frequency of the square patch depends on the coupling.

4 THZ SOURCE AND THZ CP ANTENNA

4.1 Dual-slot antenna like THz source

The dual-slot antenna is fed by discrete port Z_{port} = 10 kΩ with a parallel lumped capacitor. The photomixer exhibits a capacitive behavior The capacitance was computed from physical dimensions of the photomixer. The coordination system of the proposed antenna is shown in Fig. 4.1.

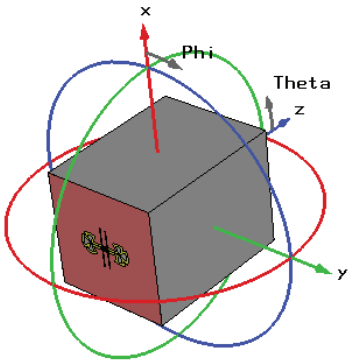

Fig. 4.1: The coordination system of the proposed antenna.

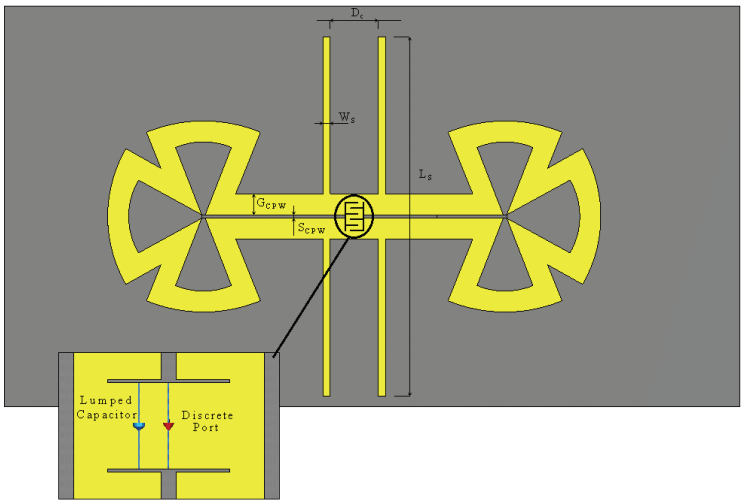

Fig. 4.2: Designed dual-slot antenna.

The designed antenna is shown in Fig. 4.2. The length of the couple of slots equals to L_S = 103 μm, the width of slots is W_S = 2 μm and thickness of metallization equals to t = 0.250 μm. The designed antenna is placed on a GaAs substrate with the thickness h_{GaAs} = 400 μm and the relative permittivity ε_{r1} = 12.94. Dealing with the coplanar waveguide (CPW) feeding line, the width of the central strip is S_{CPW} = 1 μm, the width of gaps is G_{CPW} = 6 μm and the characteristic impedance equals to Z = 89 Ω. The distance between slots in the couple is D_C = 13.76 μm. Radiation patterns of the dual-slot antenna like THz source is shown in Fig. 4.3

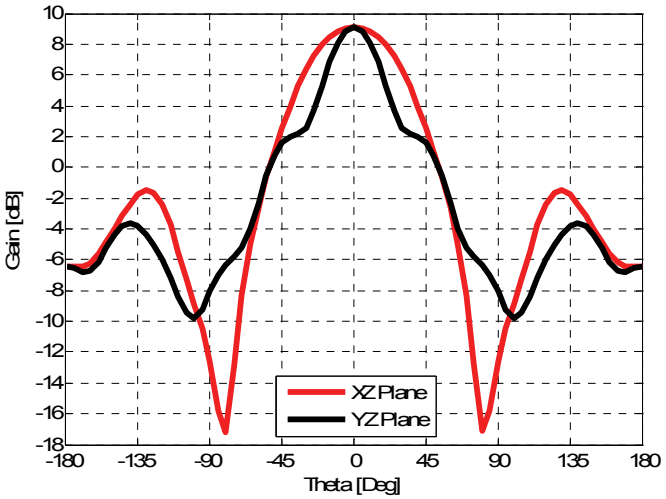

Fig. 4.3: Radiation patterns of the dual-slot antenna like THz source.

4.2 Four-leaf-clover-shaped dipole like THz source

Four-leaf-clover-shaped dipole is a special type of a full-wave dipole with bended radiating arms. The four-leaf-clover-shaped antenna [36], [37] in the full-wavelength resonance is of following parameters (see Fig. 4.4): the width L_X = 35 µm, the length L_Y = 37 µm, gaps $G_X = G_Y$ = 2 µm, and the width of the line W = 3 µm. Conductivity of the metal layer is $1.6 \cdot 10^7$ S/m and its thickness is 0.250 µm. The antenna is placed on a GaAs substrate (ε_{r1} = 12.94, h_{GaAs} = 500 µm). The line length L_{High} = 30 µm and the space G_{High} = 31 µm correspond to the high-impedance line. The line length L_{Low} = 30 µm and the space G_{Low} = 2 µm correspond to the low-impedance line. The total length of the bias line L_{Bias} = 600 µm and N = 4 repetitions are considered. Figure 4.5 shows radiation patterns of the designed structure.

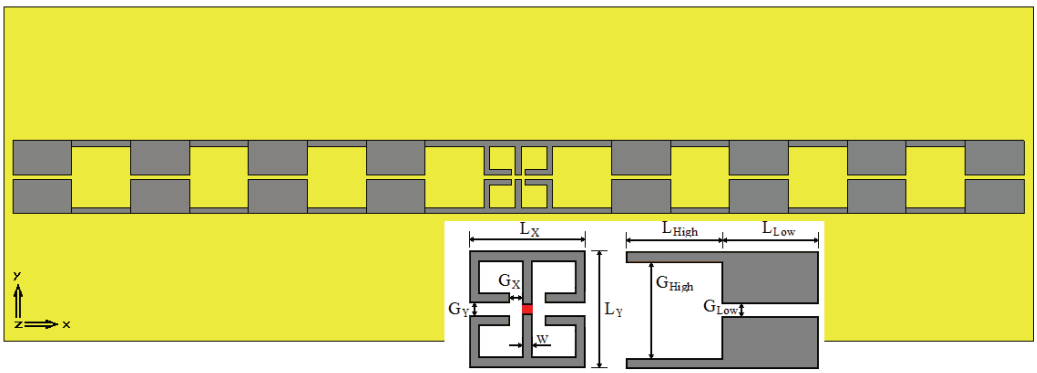

Fig. 4.4: The designed four-leaf-clover-shaped dipole antenna and biasing scheme.

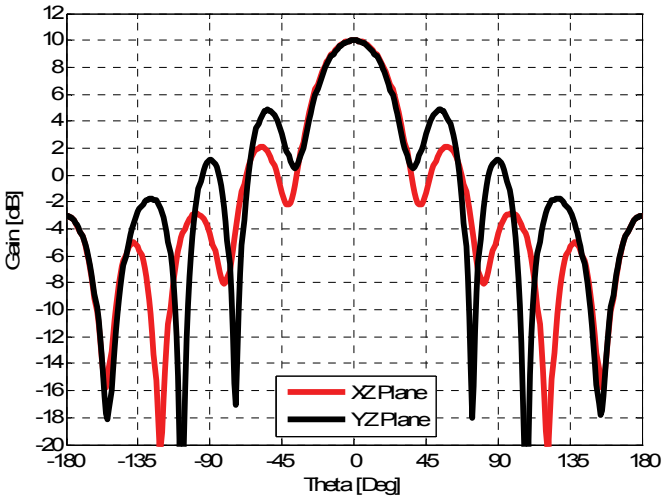

Fig 4.5: Radiation patterns of the four-leaf-clover-shaped dipole antenna like THz source.

4.3 The CP THz cross-slot patch antenna

The fundamental idea is illustrated by Fig. 4.6. The linearly polarized THz source produces THz emission. The emission passes through the GaAs substrate, and irradiates crossed slots of different lengths. The crossed slots excite two near-degenerate orthogonal modes for CP operation (TM_{10} and TM_{01}) on the radiating patch element. The square patch radiates the CP THz wave into the surrounding space. If $L_{S2}>L_{S1}$, the left-hand circular polarization can be obtained, and vice versa.

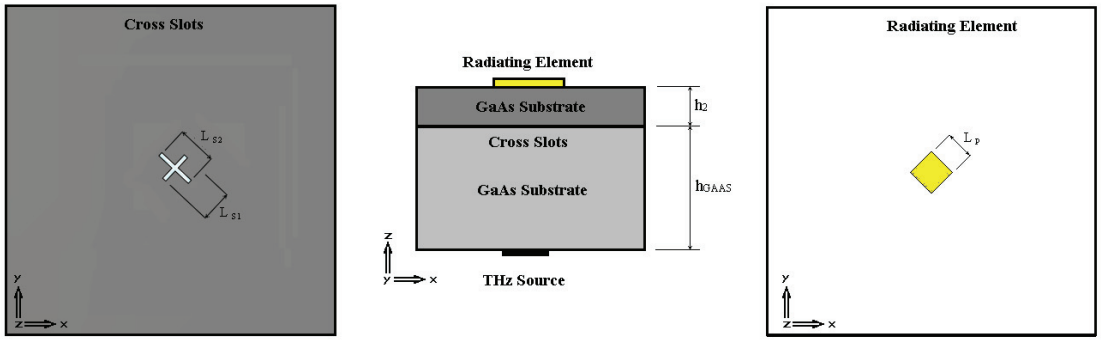

Fig. 4.6: Principle and geometry of the designed antenna.

The square patch with the side length L_P = 29.02 μm is etched on a GaAs substrate (ε_{r2} = 12.94, h_2 = 15 μm). The patch is excited via the cross-slot aperture. Lengths of arms of the cross are L_{S1} = 24.68 μm and L_{S2} = 36.05 μm. The centre of the cross and the centre of the patch have identical coordinates. Figure 4.7 shows radiation patterns of the cross-slot patch antenna in E plane and H plane. Figure 4.8 shows axial ratio of the designed antenna.

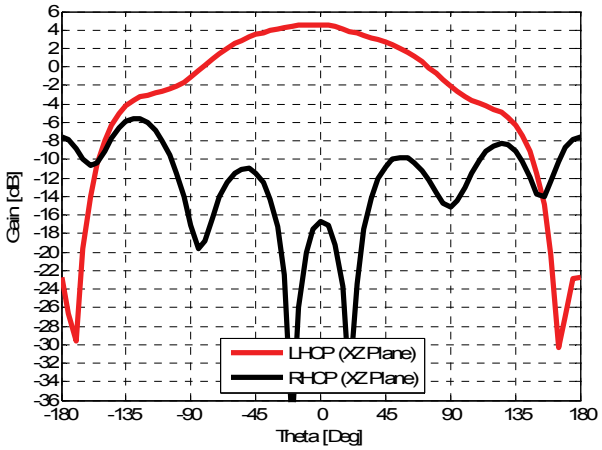

a)

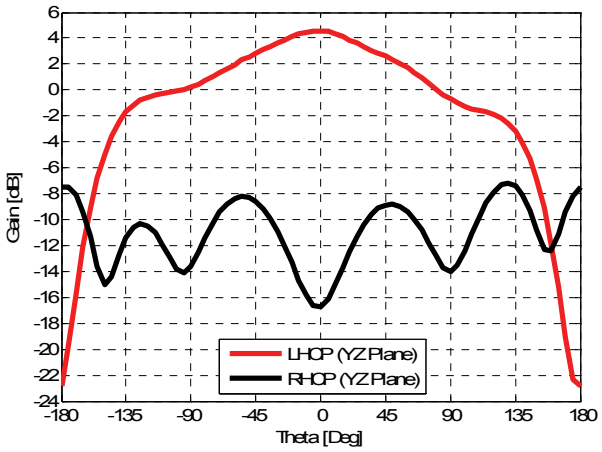

b)

Fig. 4.7: Radiation pattern of the CP THz cross-slot patch antenna, a) XZ plane, b) YZ plane.

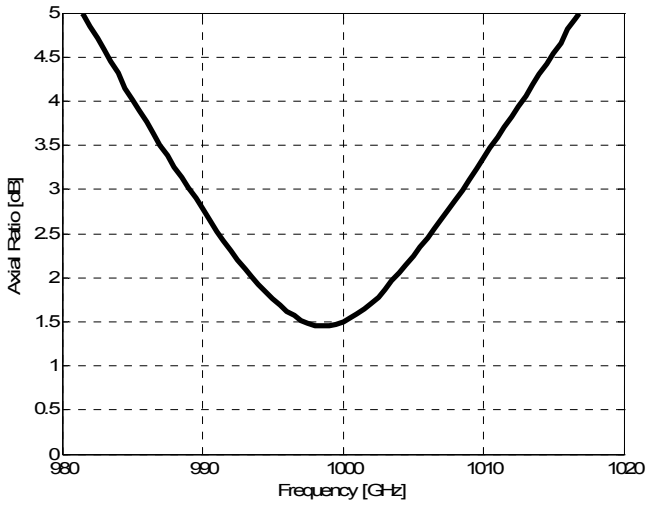

Fig. 4.8: Axial ratio in broadside direction of the CP THz cross-slot patch antenna.

5 PERIODIC STRUCTURES AND PLANAR LENS

5.1 THz mushroom-like EBG structure

Dimensions of the unit cell of the mushroom-like EBG structure are shown in Fig. 5.1. The lattice constant is D_{EBG} = 35.08 μm, the width of the patch is P_{EBG} = 19.38 μm and the width of the via is R_{EBG} = 7 μm. The gold patch with the via hole is placed on the GaAS substrate with permittivity ε_r = 12.94 and thickness h = 15 μm. The loss tangent was assumed to be 0.006. All the metal traces consisted of titanium / platinum / gold layers (thicknesses: 30 nm / 40 nm / 200 nm) in the simulation.

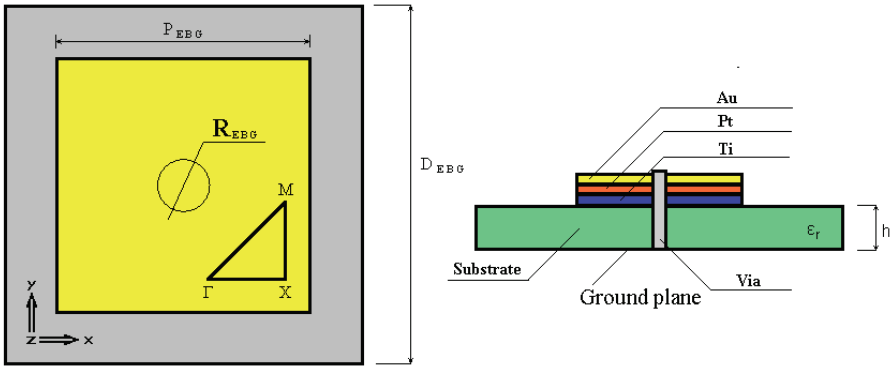

Fig. 5.1: The dimensions of the unit cell.

Fig. 5.2 shows the frequency response of the reflection phase of the mushroom-like EBG structure and the transmission of surface wave of this structure computed by CST MWS. Obviously, the EBG shows a positive reflection phase ϕ_2 = 81.77º.

Fig. 5.3 shows the dispersion diagram of the EBG. The surface wave band-gap is between 940 GHz and 1 200 GHz. The operating frequency of the CP THz cross slots patch antenna is f = 1 THz.

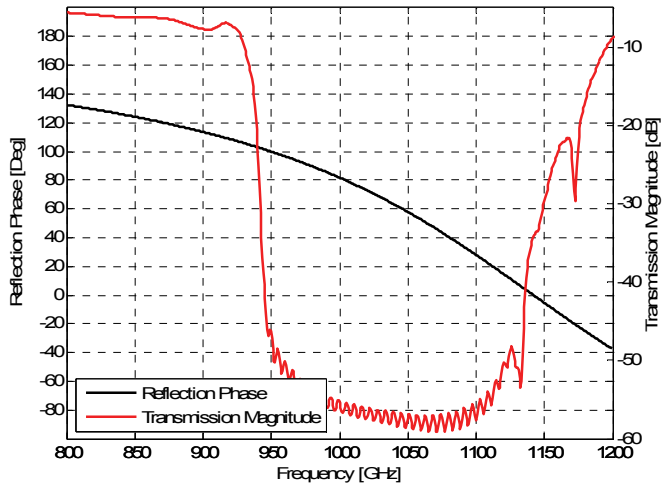

Fig. 5.2: Frequency response of reflection phase and surface wave transmission of the EBG structure.

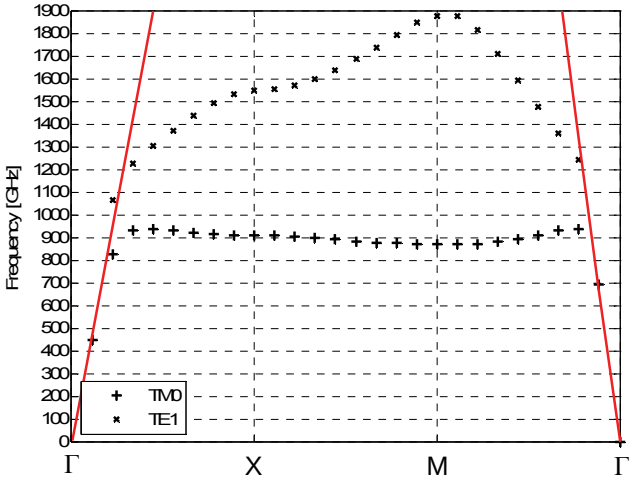

Fig. 5.3: Dispersion diagram of the mushroom-like EBG structure.

Figure 5.4 shows electric field distribution on the antenna surface and the antenna surface with mushroom-like EBG structure. Obviously, the mushroom-like EBG contributes to the suppression of surface waves and substantially improves the antenna performance.

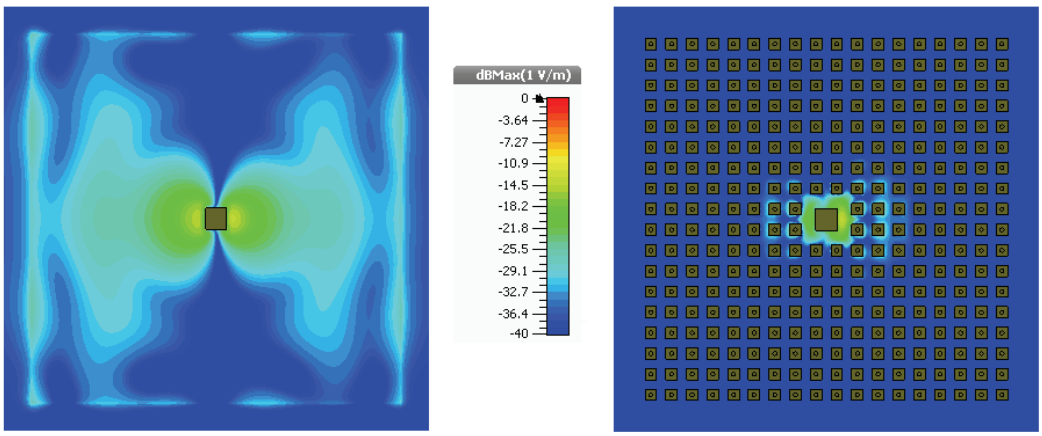

Fig. 5.4: Electric field distribution (z-component) on the antenna surface (left) and the antenna surface with mushroom-like EBG structure (right).

5.2 THz planar lenses

The principle of the superstrate antenna is explained in Fig. 5.6. The superstrate with the reflection coefficient $R_1\angle\phi_1$ is placed in the distance h_{cavity} above the ground plane. The reflection coefficient of the ground plane is $R_2\angle\phi_2$. Both reflection coefficients $R_1\angle\phi_1$ and $R_2\angle\phi_2$ are functions of the angle of incidence. For simplified ray analysis [29], we consider normal incidence only. The unit cell of a partially reflective surface (PRS, superstrate) is shown in Fig. 5.5. The unit cell is of following dimensions: D_{super} = 154.94 µm, P_{super} = 144.95 µm, ε_r = 11.9 and h_{super} = 3 µm. Here, we use higher dielectrics to achieve a high-reflecting superstrate. The superstrate was

designed for the operating frequency f = 1 THz. The antenna structure consists of a superstrate on the top and a simple radiator.

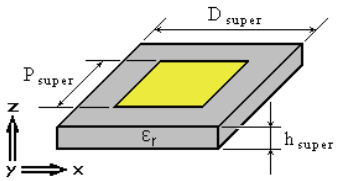

Fig. 5.5: Dimensions of the PRS unit cell.

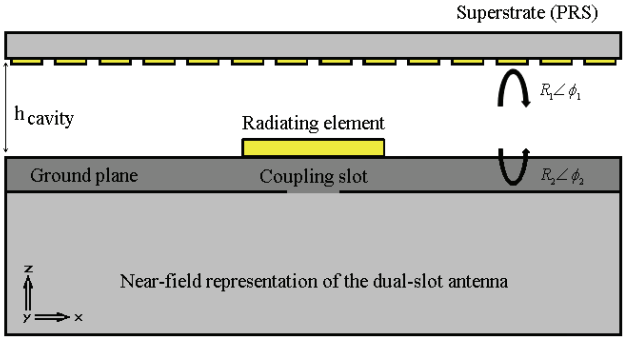

Fig. 5.6: Schematic of the superstrate antenna.

The reflection phases are very close to $\phi_1 = \phi_2 = \pi$, and the distance h_{cavity} between the ground plane and the superstrate should be $\lambda/2$ at the operating frequency

5.3 Reducing height of resonant cavity

The height of a Fabry-Perot resonator antenna is $\lambda/2$ at the operating frequency. In order to decrease the height, the reflection phase of the ground plane or the superstrate has to be changed. The difference between the partially reflective surface with a conventional ground plane and an AMC one is shown in Fig. 5.7.

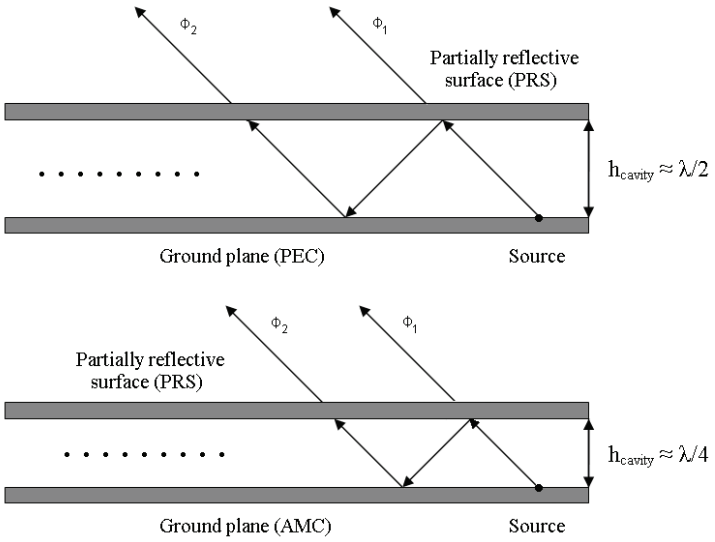

Fig. 5.7: Resonant cavity formed by PEC and PRS (top), and AMC and PRS (bottom).

5.4 THz LC superstrate like planar lens

The LC superstrate is created by a double inductive and capacitive grid. The superstrate allows us to obtain a phase shift of the reflection coefficient in between +180º and −180º. We can control the thickness of the cavity in the range between λ/2 to λ/300. The unit cell of the LC superstrate is shown in Fig. 5.7. The unit cell of the superstrate is placed on the GaAs substrate with ε_r = 12.98 and h_{super} = 15 μm (the height is high to have a high reflectiveness).

A capacitive metallic square patch is milled on one face and an inductive metallic mesh on another face of the substrate. The width of the inductive grid is W_{super} = 6.30 μm, and the width of the capacitive patch is C_{super} = 14.64 μm. Both the inductive grids and the capacitive patches have periodicity D_{super} = 17.97 μm.

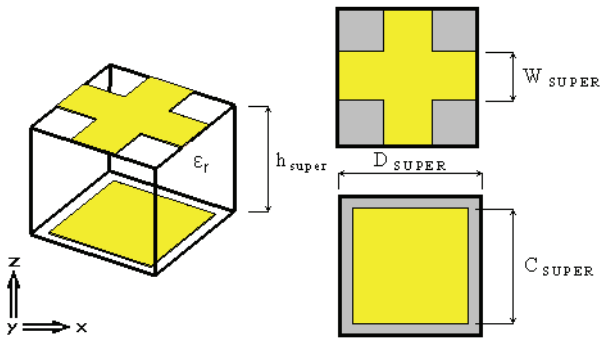

Fig. 5.7: Dimensions of the PRS unit cell.

6 FINAL THZ ANTENNA

6.1 Circularly polarized THz antenna

The structure of the antenna is shown in Fig. 6.1. Dimensions of the antenna are summarized in Table 6.1. The designed antenna is composed of four building blocks:

- The THz source: the dual slot antenna
- The CP THz cross-slot patch antenna
- The THz mushroom-like EBG structure
- The THz LC superstrate cover

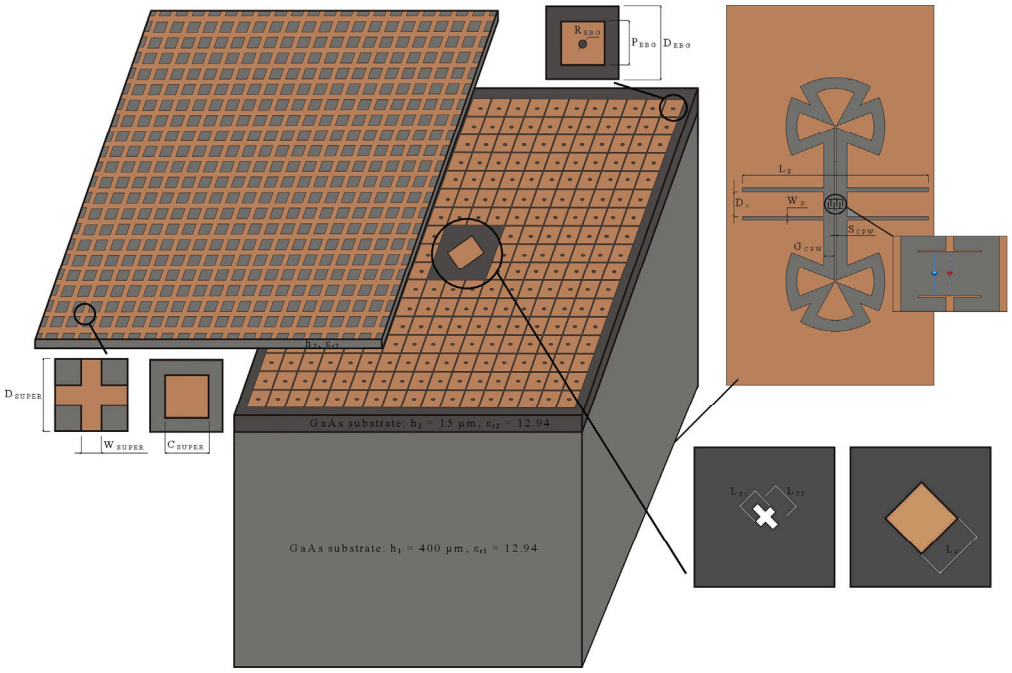

Fig. 6.1: The final THz antenna.

Table 6.1: Dimensions of the designed antenna.

Parameters	Value [μm]	Parameters	Value [μm]
h_1	400.00	G_{CPW}	6.00
ε_{r1}	12.94	S_{CPW}	1.00
h_2	15.00	D_{EBG}	35.08
ε_{r2}	12.94	P_{EBG}	19.38
L_{S1}	23.24	R_{EBG}	7.00
L_{S2}	42.45	D_{SUPER}	17.97
L_P	31.98	C_{SUPER}	14.64
L_S	103.00	W_{SUPER}	6.30
W_S	2.00	h_{cavity}	2.00
D_C	13.76	Z_{port}	10 kΩ

Fig. 6.2 shows simulated radiation patterns of the final antenna structure. In Fig. 6.3, axial ratio of the final antenna is depicted. Simulations in CST MWS show that the axial ratio bandwidth is 1.42 %. The final antenna generates left-handed circular polarization (LHCP).

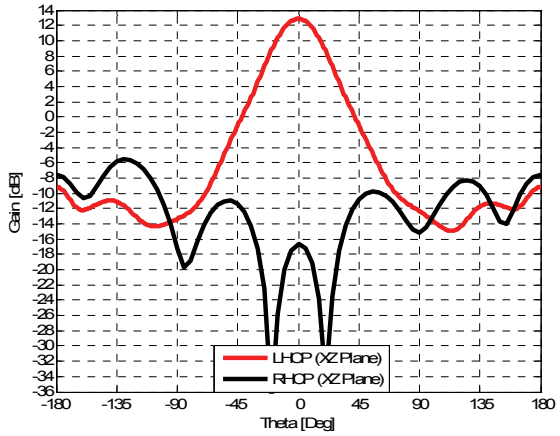

a)

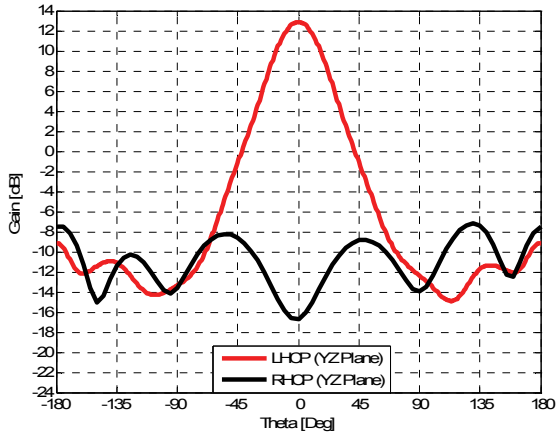

b)

Fig. 6.2: Radiation pattern of the final antenna, a) XZ plane, b) YZ plane.

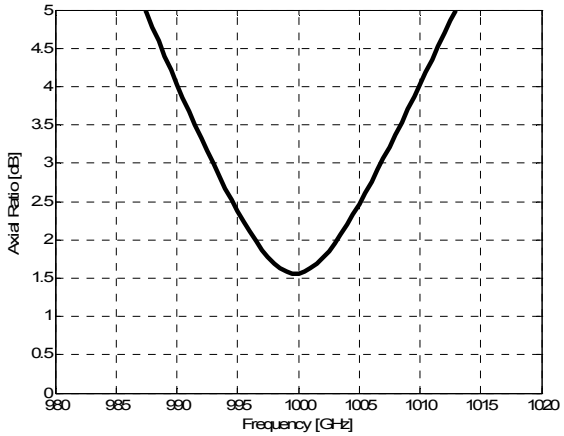

Fig. 6.3: Axial ratio in broadside direction of the final antenna.

Fig. 6.4 shows the calculated gain improvement of the final antenna. The results are summarized in the Table 6.2.

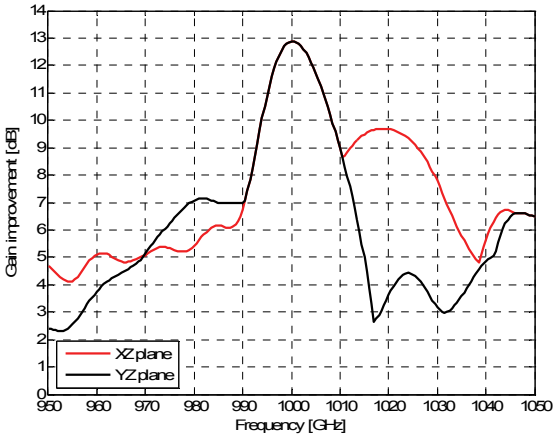

Fig. 6.4: Calculated gain improvement of the final antenna.

Table 6.2: Simulation results for basic antenna and final one.

Results for f = 1 THz, cavity = λ/150	**Basic antenna**	**Final antenna**
SSL, XZ plane	-5.9 dB	-22.0 dB
SSL, YZ plane	-5.5 dB	-19.3 dB
FBR, XZ plane	6.2 dB	22.0 dB
FBR, YZ plane	5.5 dB	18.5 dB
Main lobe width, XZ plane	132.4°	33.8º
Main lobe width, YZ plane	136.1°	40.7º
Gain, XZ plane	4.6 dB	13.0 dB/14.8 dB*
Gain, YZ plane	4.6 dB	13.0 dB/14.8 dB*
Gain improvement	0.0 dB	8.4 dB/10.2 dB*
Axial ratio	2.0 %	1.4 %
Radiation efficiency	57.5 %**	50.7 %**

(*) Theoretical value calculated from complex reflection coefficient, (**) Calculated by CST MWS for a conventional antenna without optical conversion.

6.2 Experimental verification at f = 10 GHz

The final antenna consists of the LC superstrate, mushroom-like EBG ground plane and CP cross-slot patch antenna. The feeding was implemented by microstrip transmission line. Structure of the antenna is shown in Fig. 6.5.

The square patch of a side length L_P = 6.17 mm with metallization t = 0.035 mm is etched on a substrate with the thickness h_2 = 0.762 mm and the relative permittivity ε_{r2} = 3.38. The microstrip feeding line is of characteristic impedance Z_0 = 50 Ω. The matching line L_{OS} = 1.40 mm is etched on a substrate with the thickness h_1 = 1.016 mm and the relative permittivity ε_{r1} = 10.2. The patch is excited via the cross-slot aperture. Lengths of arms of the cross are L_{S1} = 4.06 mm and L_{S2} = 3.66 mm. The center of the cross and the center of the patch have identical coordinates.

The dimensions of the mushroom-like EBG are periodicity D_{EBG} = 4.63 mm, the width of the patch P_{EBG} = 4.33 mm and the radius of via R_{EBG} = 0.6 mm.

Fig. 6.6 shows frequency response of the reflection phase of the mushroom-like EBG and surface wave transmission of the mushroom-like EBG computed by CST MWS (the EBG has a positive reflection phase ϕ_2 = 136.96º).

Fig. 6.7 shows the dispersion diagram of EBG. The band-gap is from 9.23 GHz to 10.70 GHz. Operating frequency is f = 10 GHz. The EBG consists of 17×17 unit cells.

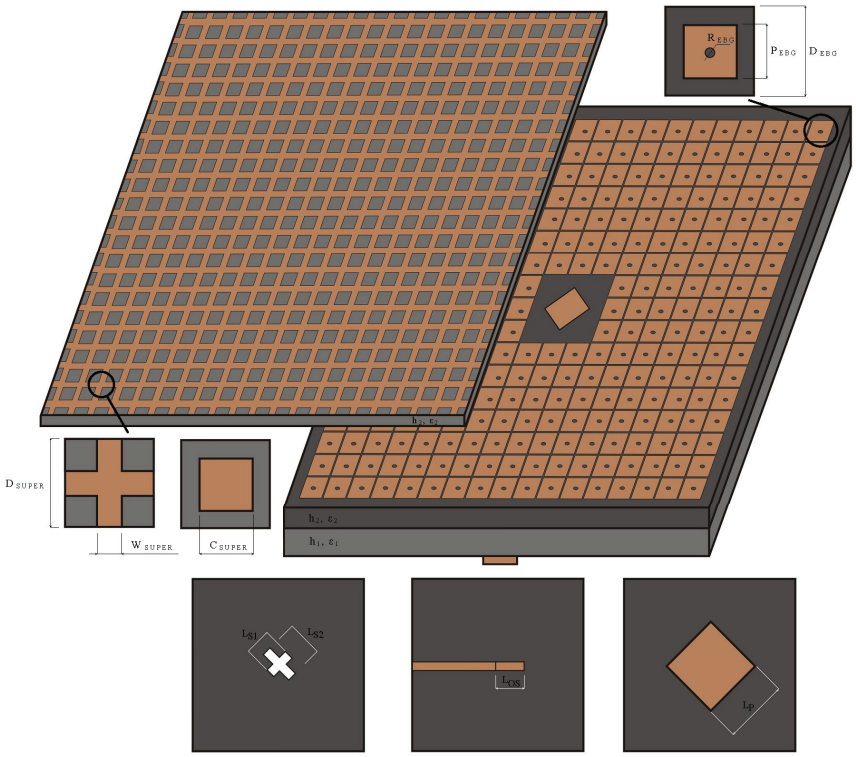

Fig. 6.5: Geometry of the final structure.

In Figure 6.9, computed and measured frequency responses of reflection coefficient are compared. The impedance bandwidth of the measured antenna is 2.57%.

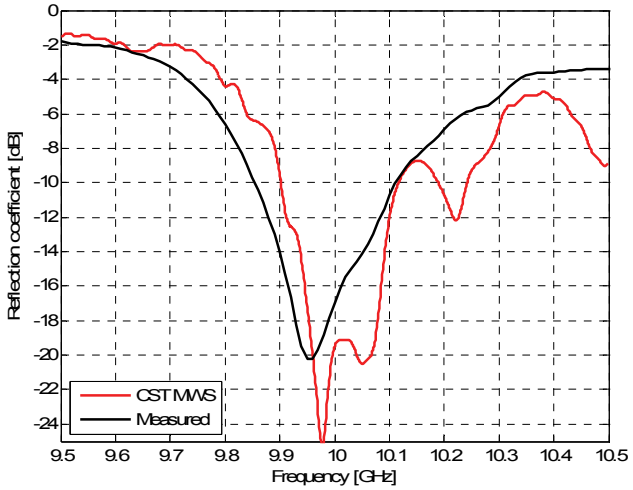

Fig. 6.9: Simulated and measured reflection coefficient of the final antenna.

In Figure 6.10, computed and measured axial ratio in broadside direction is given. The axial ratio bandwidth is 0.6% against 1.9% achieved by CST MWS. Axial ratio strongly depends on the composition of each layer. In this case, the final antenna was set for generating the left-handed circular polarization (LHCP).

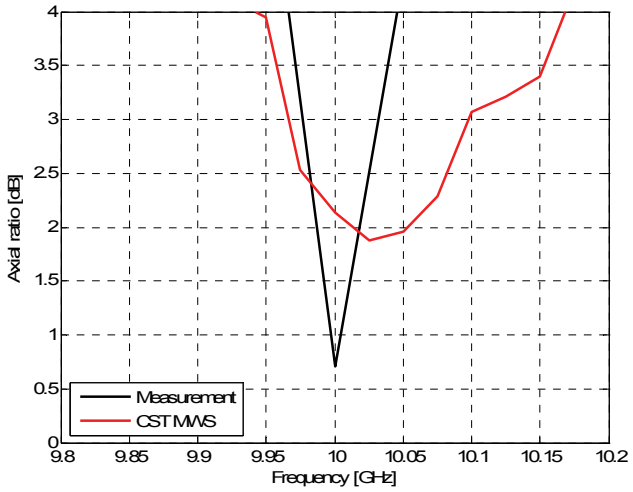

Fig. 6.10: Measured axial ratio of the final antenna.

Figure 6.11 shows simulated and measured radiation patterns at the center frequency.

Thanks to the band-gap, the mushroom-like EBG structure can suppress surface waves and reduce the side lobe level. The results show smoother radiation patterns with smaller wasted power in the backward hemisphere. The comparison of the basic CP antenna (without EBG and superstrate, ground plane dimensions 83 mm × 83 mm) with the final simulated structure and measurements are shown in Table 6.3.

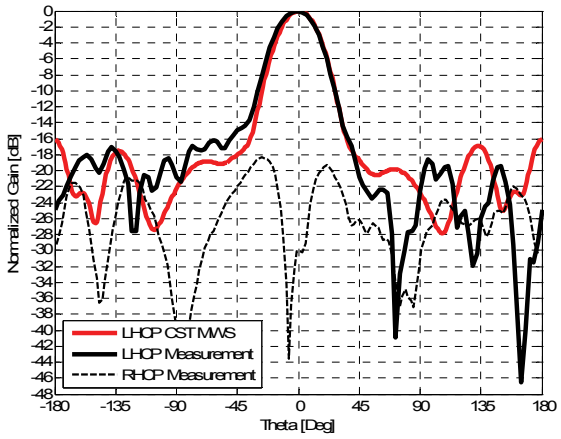

a)

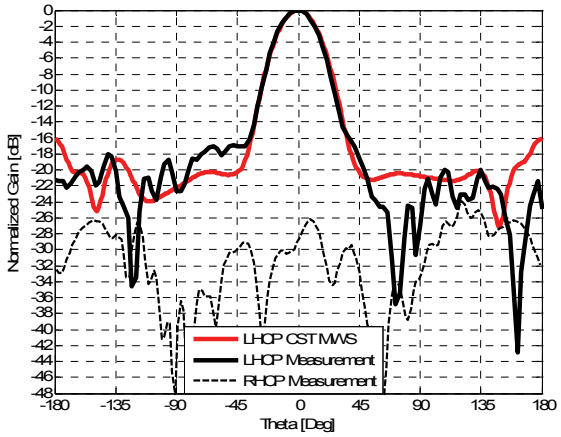

b)

Fig. 6.11: Radiation patterns of fabricated antenna at 10 GHz a) XZ plane, b) YZ plane.

Table. 6.3: Simulation and measurement results for final antenna.

Results for f = 10 GHz	**Basic**	**Final: Simulation**	**Final: Measurement**
SSL, XZ plane	-11.9 dB	-21.7 dB	-18.7 dB
SSL, YZ plane	-12.4 dB	-20.8 dB	-18.5 dB
FBR, XZ plane	13.6 dB	29.3 dB	24.2 dB
FBR, YZ plane	13.6 dB	29.3 dB	21.2 dB
S_{11} bandwidth	4.0%	2.1 %	2.6 %
AR bandwidth (3 dB)	2.1 %	1.9 %	0.6 %
Cavity height	none	λ/22	λ/22
Main lobe width, XZ plane	110.2º	25.6º	14.6º
Main lobe width, YZ plane	117.0º	26.6º	14.6º
Gain, XZ plane	5.3 dB	16.0 dB	16.0 dB
Gain, YZ plane	5.3 dB	16.0 dB	16.0 dB
Gain improvement	0.0 dB	10.7 dB	10.7 dB

7 CONCLUSION

The thesis was focused on the design and modelling of circularly polarized THz antenna with circular polarization. The thesis contributed to the solution of following problems:

- We developed a technique for calculating the parasitic capacitance of the photoconductive mixer which respects the geometry of electrodes and the substrate.
- We designed a dual-slot antenna and a four-leaf-clover-shaped dipole. The four-leaf-clover-shaped dipole exhibited very high input impedance, which is suitable for the connection to the LT-GaAs photomixer.
- We designed a planar lens to focus the radiated energy into the main lobe and suppress the level of side lobes.
- We completed the final prototype of the circularly polarized antenna and verified its functionality by simulations and measurements.

The numerical results are summarized in the following table:

Dual-slot antenna (like THz source)	**Value**
Main lobe magnitude	9.1 dB
Side lobe level, XZ Plane	-10.6 dB
Side lobe level, YZ Plane	-12.8 dB
Angular width (3 dB), XZ Plane	62.4°
Angular width (3 dB), YZ Plane	34.8°
Radiation efficiency	61.4 %
Four-leaf-clover-shaped dipole	**Value**
Main lobe magnitude	10.0 dB
Side lobe level, XZ Plane	-7.6 dB
Side lobe level, YZ Plane	-5.1 dB
Angular width (3 dB), XZ Plane	44.2°
Angular width (3 dB), YZ Plane	42.3°
Radiation efficiency	91.9 %
CP THz antenna with THz source	**Value**
Main lobe magnitude	4.6 dB
Side lobe level, XZ Plane	-5.9 dB
Side lobe level, YZ Plane	-5.5 dB
Angular width (3 dB), XZ Plane	132.4°
Angular width (3 dB), YZ Plane	136.1°
Radiation efficiency	77.7 %

Second, the effort was aimed to exploit periodic structures for the implementation of a planar lens and an electromagnetic band gap substrate:

- We developed a method for correct design of periodic structures. We dealt with a mushroom-like EBG structure: the design method was developed, and experiment confirmed results. Surface waves were suppressed and antenna parameters were improved.
- We created two types planar lenses: (1) a conventional superstrate and (2) a novel LC superstrate. The LC superstrate allows the reduction of the height of the resonant cavity at minimum.

Finally, we experimentally verified described principles at 10 GHz. The designed structure affirmed the correctness of the concept and improvement of antenna parameters.

Now I would like to compare the advantages and disadvantages of my design with a conventional concept.

My design (advantages):

Circular polarization, small dimensions, planar structure, single superstrate for antenna matrix, small mutual coupling between antenna elements, side lobe level suppression, improvement of front to back ratio.

My design (disadvantages):

Complicated design, radiation efficiency, narrowband structure, losses in high permittivity dielectrics, skin effect.

Conventional concept (advantages):

Wideband and narrowband structures, high gain (directivity), easy to fabricate.

Conventional concept (disadvantages):

Large dimensions, each antenna element needs a silicon lens, intricately connection between the antenna and lens.

REFERENCES

[1] SIEGEL, P. Terahertz technology. *IEEE Transactions on Microwave Theory and Techniques*. 2002, vol. 50, no. 3, page 910 - 928.

[2] EICHHORN, F. *Ultrabroadband Photonic Receiver Concepts for Terahertz Frequencies*. Master's thesis, Denmmar: Technical University of Denmark, 2006.

[3] CROWE, T., BISHOP, W., PORTERFIELD, D., HESLER, J., WEIKLE, R. M. Opening the terahertz window with integrated diode circuits. *IEEE Journal of Solid-State Circuits.* 2005, vol. 40, no. 10, page 2104 - 2110.

[4] LOATA, G. *Investigation of low-temperature-grown GaAs photoconductive antennae for continous-wave and pulsed terahertz generation*. Dissertation thesis, Germany: Vorgelegt beim Fachbereich Physik der Johann Wolfgang Goethe-Universität in Frankfurt am Main, 2007.

[5] BROWN, E. R., WILD, W., CUNNINGHAM, C. Alma The Atacama Large Millimeter Array. *Advances in Space Research. 2004*, vol. 34, no. 3, page 555 - 559.

[6] PHILLIPS, T., KEENE, J. Submillimeter Astronomy Heterodyne Spectroscopy. In *Proceedings of the IEEE*. 1992, vol. 80, no. 11, page 1662 - 1678.

[7] LOER, T., SIEBERTT, K. J., HASAGAWA, N., HAHN, T., LOATA, G., WIPF, R., KRESS, M., THOMSON, M., ROSKOS, H. G. Terahertz Surface and Interface Characterization. *IEEE MTT-S International Microwave Symposium Digest*. 2005, pages 4.

[8] FERGUSON, B., WANG, S., GRAY, D., ABBOTT, D., ZHANG, X-C. Towards Functional 3D T-ray Imaging. *Physics in Medicine and Biology*. 2002, vol. 47, page 3735 - 3742.

[9] WALLACE, V. P., PICKWELL, E., FITZGERALD, A. J., PINDER, S. Terahertz Pulsed Imaging and Spectroscopy of Breast Tumours. *14th International Conference on Teraherz Electronics and Infrared Millimeter Waves. 2006,* page 585 - 585.

[10] TRIBE, W. R., NENHAM, P. A., TADAY P. F., KEMP, M. C. Hidden Object Detection: Security Applications of Terahertz Technology. *Proceedings of Terahertz and Gigahertz Electronics and Photonics.* 2004 vol. 53, no. 54, page 168 - 176.

[11] LEAHY-HOPPA, M. R., FITCH, M. J., ZHENG, X., HAYDEN, L. M., OSIANDER, R. Wideband Terahertz Spectroscopy of Explosives. *Chemical Physics Letters.* 2007 no. 434, vol. 50, page 227 - 230.

[12] SYDLO, C., SIGMUND, J., FEIGIMOV, M, MEISSNER, P. HARTNAGEL, H. L. Coherent Generation and Detection of Continuous THz Waves Using Two Photomixers Driven by Laser Diodes. *Conference Digest of the 2004 Joint 29th International Conference on Infrared and Millimeter Waves and 12th International Conference on Terahertz Electronics. 2004,* page 200 - 201.

[13] SASAKI, Y., SUIZU, K., ITO, H. Surface-emitted Terahertz-wave Generation Using Double Injection Seeded Optical Parametric Generation. *The 5th Pacific Rim Conference on Lasers and Electro-Optics,* 2003.

[14] BROWN, E. R. THz Photomixing. *The 20th Annual Meeting of the IEEE Lasers and Electro-Optics Societ., 2007,* page 790 - 791.

[15] BROWN, E. R. Thz Generation by Photomixing in Ultrafast Photoconductors. *International Journal of High Speed Electronics and System. 2003,* vol. 13, no. 2, page 497 - 545.

[16] FRITSCHE C. *Design and Modeling of an Ultrafast Broadband Photonic Mixer*. Master's thesis, Denmark: Technical University of Denmark, 2005.

[17] RENNER, F., ECKARDT M., SCHWANHAUSSER, A., KLAR, O., MALZER., S., DOHLER, G., LOATA, G., LOFFLER, T., ROSKOS, H., HANSON, M., DRISCROLL, D, GOSSARD, A. Thz-emitter Based on Ballistic Transport in nano-pin Diodes. *Physica Status Solidi (A) Applied Research*. 2005, page 965 - 969.

[18] ITO, H., KODAMA, S., MURAMOTO, Y., FURUTA. T., NAGATSUMA, T., ISHIBASHI, T. High-speed and high-output inp-ingaas Unitraveling-carrier Photodiodes. *IEEE Journal of Selected Topics in Quantum Electronics. 2004*, vol. 10, no. 4, page 709 - 727.

[19] FRITSCHE, C., KROZER, V. Large-signal Pin Diode Model for Ultra-fast Photodetectors. *35th European Microwave Conference - Paris*. 2005.

[20] ZEDLER, M., HARING-BOLIVAR, P., KURZ, H. Improved coherent THz emission by modification of the dielectric environment. *Quantum Electronics and Laser Science*, 2003.

[21] DOWN, A., WHITTAKER, D. M., CORCHIA, A., DAVIES, A.G., LINFIELD, E.H. Enhancement of THz emission from semiconductor surfaces. *Tenth International Conference on Terahertz Electronics Proceedings. 2002,* page 48 - 51.

[22] ITO, H., FURUTA, T., NAKAJIMA, F., YOSHINO, K., ISHIBASH, T. Photonic Generation of Continuous THz Wave Using Uni-Traveling-Carrier Photodiode. *Lightwave Technology. 2005, vol. 23 , no. 12*, page 4016 - 4021.

[23] ITO, H., ISHIBASH, T. Ultrafast Uni-Traveling Carrier Photodiode. *58th Conference Device Research Conferenc. 2000*, page 165 - 168.

[24] STUZTAN, W. L., THIELE G. A. *Antenna Theory and Design*, John Willey & Sons, 1998. ISBN-13: 978-0470576649.

[25] MILLIGAN, T. A. *Modern Antenna Design*. New Jersey: John Willey & Sons, 2005. ISBN-13: 978-0471457763.

[26] MENDIS, R., SYDLO, C., SIGMUND, J., FEIGINOV, M., MEISSNER, P., HARTNAGEL, H. L. Spectral Characterization of Broadband Thz Antennas by Photoconductive Mixing: Toward Optimal Antenna Design. *IEEE Antennas and Wireless Propagation Letters*. 2005, vol. 4, no. 1, page 85 - 88.

[27] KAZIM, M. I. *Design of Continuous-Wave Photonic TeraHertz*. Antennas Master's thesis, Denmmar: Technical University of Denmark, 2006.

[28] WOO, I., NGUYEN T.K., HAN, H., LIM, H., PARK, I. Four-leaf-clover-shaped antenna for a THz photomixer, *Optics Express*, Vol. 18, Issue 18, 2010 page 18532-18542.

[29] PITRA, K.; KOVACS, P.; RAIDA, Z.; HARTNAGEL, H. Design of Circularly Polarized Terahertz Antenna with Superstrate (Cover) Layer. *In Proceedings of the International Conference on Electromagnetics in Advanced Applications(ICEAA)*. 15. Torino, Italy, 2013. page 363-363.

CURRICULUM VITAE

Name: Kamil Pítra

Born: April 2nd 1984 in Strakonice, Czech Republic

Contact: kamil.pitra@seznam.cz

Education:

2010 - 2014 Brno University of Technology /Department of Radio Electronics
Doctoral's degree, Electronics and Communications
Thesis: (Sub)millimeter-wave antennas

2008 - 2010 Brno University of Technology / Department of Radio Electronics
Master's degree, Electronics and Communications
Thesis: Antennas for millimeter-wave bands

2005 - 2008 Brno University of Technology /Department of Radio Electronics
Bachelor's degree, Electronics and Communications
Thesis: Low altitude FM radio-altimeter

Experience:

10/2013 to 11/2013 TU Darmstadt (Prof. Hartnagel), Germany
Study stay: Analysis and design of antennas for THz frequency band.

3/2013 to 5/2013 TU Darmstadt (Prof. Hartnagel), Germany
Study stay: Analysis and design of antennas for THz frequency band.

11/2013 to 12/2011 TU Darmstadt (Prof. Hartnagel), Germany
Study stay: Analysis and design of antennas for THz frequency band.

Languages:

Czech, English

Specialization:

Analysis and design of antennas, modelling and simulation of microwave and RF structures, antenna measurement

ABSTRACT

The thesis deals with the design and optimization of circularly polarized antennas for THz frequencies. In the thesis, a simplified theory of THz sources is presented, and a suitable antenna for a THz source is designed. The design is focused on achieving circular polarization from linearly polarized antennas. In order to suppress surface waves on an electrically dense dielectric substrate, we design and optimize specific periodic structures. The design of such a structure is rather complicated since the relation between electromagnetic band gap (EBG) properties and unit cell geometry is not straightforward. In order to properly focus the radiated energy, we design and optimize a partially reflective surface (PRS) acting as a planar lens for the THz antenna.